Acta Pharmaceutica Sinica B 2019;9(3):604–614

Chinese Pharmaceutical Association
Institute of Materia Medica, Chinese Academy of Medical Sciences

Acta Pharmaceutica Sinica B

www.elsevier.com/locate/apsb
www.sciencedirect.com

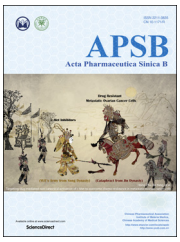

ORIGINAL ARTICLE

Prussian blue nanosphere-embedded *in situ* hydrogel for photothermal therapy by peritumoral administration

Jijun Fu[a,b], Bo Wu[a,c], Minyan Wei[b], Yugang Huang[a,b], Yi Zhou[a,b], Qiang Zhang[b,*], Lingran Du[b,*]

[a]*The Fifth Affiliated Hospital of Guangzhou Medical University, Guangzhou Medical University, Guangzhou 510700, China*
[b]*Key Laboratory of Molecular Target & Clinical Pharmacology, School of Pharmaceutical Sciences, Guangzhou Medical University, Guangzhou 511436, China*
[c]*Center of Pharmaceutical Research and Development, School of Pharmaceutical Sciences, Guangzhou Medical University, Guangzhou 511436, China*

Received 22 August 2018; received in revised form 23 October 2018; accepted 30 October 2018

KEYWORDS

Prussian blue;
Nanospheres;
Hydrogel;
Thermosensitive;
Injectable;
In situ;
Photothermal

Abstract To establish an injectable hydrogel containing Prussian blue (PB) nanospheres for photothermal therapy against cancer, PB nanospheres were prepared by one-pot synthesis and the thermosensitive Pluronic F127 was used as the hydrogel matrix. The PB nanospheres and the hydrogel were characterized by shape, particle size, serum stability, photothermal performance upon repeated 808 nm laser irradiation, as well as the rheological features. The effect of the PB nanospheres and the hydrogel were evaluated qualitatively and quantitatively in 4T1 mouse breast cancer cells. The retention, photothermal efficacy, therapeutic effects and systemic toxicity of the hydrogel were assessed in a tumor-bearing mouse model. The PB nanospheres had a diameter of about 150 nm and exhibited satisfactory serum stability, photo-heat convert ability and repeated laser exposure stability. The hydrogel encapsulation did not negatively influence the above features of the photothermal agent. The nanosphere-containing hydrogel showed a phase transition at body temperature and, as a result, a long retention time *in vivo*. The photothermal agent-embedded hydrogel displayed promising photothermal therapeutic effects in the tumor-bearing mouse model with little-to-no systemic toxicity after peritumoral administration.

*Corresponding authors.
E-mail addresses: zqdodo@bjmu.edu.cn (Qiang Zhang), dulingran@126.com (Lingran Du).

Peer review under responsibility of Institute of Materia Medica, Chinese Academy of Medical Sciences and Chinese Pharmaceutical Association.

https://doi.org/10.1016/j.apsb.2018.12.005

1. Introduction

In the past few years the world has witnessed many new methods in treating cancers[1–10], such as monoclonal antibodies, gene therapy[4,10], photodynamic therapy (PDT), sonodynamic therapy, and photothermal therapy (PTT)[8]. However, cancer therapy is still a big challenge, with the mean survival length of cancer patients only several years.

As a traditional dosage form, hydrogel has been extensively investigated in many research fields, especially in regeneration medicine. For example, murine adipose-derived stem cells could be easily loaded into poly(ethylene glycol)-gelatin hydrogel and maintained their characteristics and enhanced angiogenesis and wound healing[11]. Proteins or peptides were also reported to be able to form promising hydrogels[12–14]. To improve the survival of endothelial progenitor cells in hydrogels, tacrolimus was embedded into RADA16 hydrogel as an immunosuppressant to reduce immune rejection of the stem cells[15]. Nonsteroidal anti-inflammatory drug-modified D-tetrapeptides ($G^DF^DF^DY$) were used to construct an OVA antigen-loaded hydrogel, which provided a superior immune-stimulating effect due to reduced inflammatory responses[16]. A unique fast-swelling polycation hydrogel was suggested to behave as an antimicrobial super-absorber with long lasting antimicrobial ability due to interactions between the cationic surface of the hydrogel and the negatively charged microbe[17]. Application of hydrogels in treating cancers is also a newly emerging research field. Carboxymethyl cellulose-modified PNIPAAmMA hydrogel was used to carry epirubicin and paclitaxel nanoparticles and the hydrogel system showed satisfactory performance in preventing brain tumor recurrence[18]. Hydrogel formed by alginate-*g*-poly(*N*-isopropylacrylamide) was reported to be able to release doxorubicin-loaded micelles[19].

There has been increasingly widespread interest in PTT. The photothermal agents (PTAs) are able to convert laser energy, especially near-infrared light (NIR) which can penetrate deep into tissues, into heat energy. PTT is often used to treat cancers. $CuCo_2S_4$ nanocrystals are newly discovered photoacoustic imaging (PAI) and magnetic resonance imaging (MRI)-guided PTAs[20]. Core-shell Gd-tailored gold nanorods (GNR) were used for multimodal imaging guided PTT[21]. A MnO_2 functionalized Co-P nanocomposite is a promising candidate to be used for synergistic chemo-photothermal therapy[22]. Jiang et al.[23] embedded a PTA, melanin, into biomimetic nanoparticles composed of red blood cell membranes and the system showed satisfactory photothermal therapeutic effects due to the long circulation time of the biomimetic vehicles and the enhanced penetration and retention effects (EPR) of tumor tissues.

Normally, PTAs are administered intravenously. Despite great advances in PTT, the toxicity of the intravenous administered PTAs remains a big concern as most of the PTAs are made of heavy metal elements, such as gold and bismuth. In addition, despite the EPR and other targeting methods, the nano-carriers final distribution into tumor tissues accounts for only a small proportion of the total dose administered; as a result, the limited tumor distribution limits therapeutic effects and increases systemic toxicity. In this study, an injectable Pluronic F127 hydrogel containing Prussian blue (PB) nanospheres for peritumoural administration is proposed (Fig. 1). As the hydrogel is locally administered and has a long retention time, it is believed that this system will exhibit better photothermal therapeutic effects and reduced systemic toxicity.

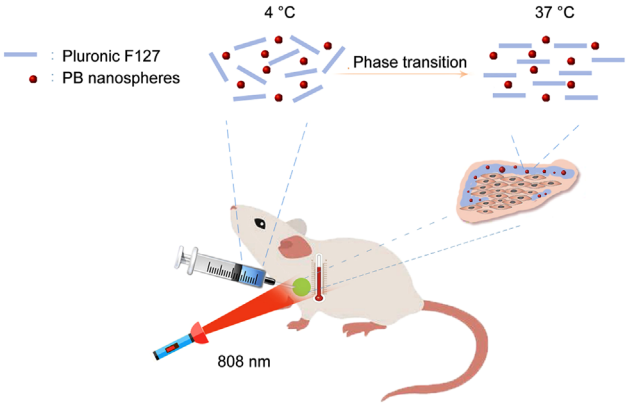

Figure 1 Schematic illustration.

2. Materials and methods

2.1. Preparation and characterization of PB nanospheres

One hundred milligram of polyvinylpyrrolidone (MW 24,000) was added into 10 mL of 0.01 mol/L HCl solution and the mixture was stirred until clear. Then, 33 mg of $K_3Fe(CN)_6$ was added with stirring. The solution was heated to 80 °C for 12 h with stirring to yield blue nanodispersions. After dialysis in pure water, PB nanospheres were obtained. The appearance of the nanospheres were imaged by transmission electron microscopy (TEM, 100 kV) and particle size was measured by a particle-sizing system (Malvern, UK).

To investigate the stability of the PB nanospheres, serum was added to PB nanodispersions to a final concentration of 10%, with the concentration of PB nanospheres at 0.2 mg/mL. The sample was placed in a water bath at 37 °C for 3 days and the particle size of the nanospheres before and after storage was measured.

To evaluate the photothermal performance of PB nanospheres, the nanodispersions with different concentrations (0, 100, 200, and 400 μg/mL) were exposed to 808 nm laser at 1 W/cm^2. Temperatures of the samples at different time points were recorded by infrared imaging (Fotric).

To further characterize the PB nanospheres, the sample with 0.2 mg/mL PB was exposed to NIR irradiation for five cycles. After each irradiation for 5 min at 1 W/cm^2, the sample was cooled to room temperature and then exposed to the 808 nm laser again. The temperature of the samples was monitored. Particle size and visible absorption curves of the sample before and after the 5-cycle irradiation were measured.

2.2. Preparation and characterization of PB nanospheres embedded Pluronic F127 hydrogel

Pluronic F127 granules were added to PB nanodispersions with stirring in an ice bath to produce the PB nanosphere-loaded hydrogel. The concentration of Pluronic F127 was 0.2 g/mL, and the concentration of PB nanospheres was 0.25 mg/mL.

Hydrogel loaded with PB nanospheres was frozen in liquid nitrogen overnight and then the frozen hydrogel was lyophilized. The shape of the final sample was imaged by scanning electron microscopy (3.0 kV). Blank Pluronic F127 hydrogel was used as a control.

To investigate the photothermal performance of the PB nanosphere-loaded hydrogel, the hydrogel was exposed to the 808 nm laser at 1 W/cm^2. The temperature of the hydrogel at different times was monitored. Blank hydrogel was used as a control.

To further characterize the PB nanosphere-loaded hydrogel, the rheological features of the samples were determined. The frequency was 1 Hz, and the heating rate was 1 °C /min. A blank hydrogel was used as a control.

To study the stability of the PB nanosphere-loaded hydrogel, the sample was placed at 37 °C for 15 days. The hydrogel sample before and after storage was diluted with water 10-fold and then measured by the particle sizing system to determine the size of the PB nanospheres. The heating curves upon NIR irradiation (808 nm, 1 W/cm^2) were determined before and after different storage times. The similarity between two curves was evaluated by f_2 factor according to Eq. (1), and $f_2 > 50$ means highly similar.

$$f_2 = 50\log_{10}\left\{\left[1+\frac{1}{n}\sum_{i=1}^{n} W_t\left(\overline{R}_t-\overline{T}_t\right)^2\right]^{-0.5}\times 100\right\} \quad (1)$$

where R_t and T_t indicate temperature of the sample before and after storage upon NIR irradiation at t (min).

2.3. Assessment of in vitro photothermal therapeutic effects

The 4T1 mouse breast cancer cells (1×10^4) were seeded in 96-well plates and incubated overnight (37 °C, 5% CO_2). The next morning PB nanodispersions were added to make the final concentration of the nanospheres 0, 2, 5, 10, 20, 50, 100, and 200 μg/mL. The cells were incubated for another 24 h and then exposed to the 808 nm laser (1 W/cm^2) for 1 min. Cells not receiving NIR treatment were used as a control. After incubation for another 4 h, the viability of the cells was measured by the MTT method.

L02 hepatic cells (1×10^4) were seeded in 96-well plates and incubated overnight (37 °C, 5% CO_2). PB nanodispersions then were added to make final concentration of the nanospheres 0, 2, 5, 10, 20, 50, 100, and 200 μg/mL. The cells were incubated for another 24 h. The viability of the cells was measured by MTT method.

4T1 mouse breast cancer cells (5×10^4) were seeded in 24-well plates and incubated overnight (37 °C, 5% CO_2). PB nanodispersions then were added to make the final concentration of the nanospheres 50 μg/mL. The cells were exposed to the 808 nm laser (1 W/cm^2) for 3 min; cells treated with PBS and the cells not receiving NIR treatment were used as controls. After incubation for another 4 h, propidium iodide (final concentration 30 μg/mL) was added and incubated for 30 min to stain the dead cells. The culture media was discarded and the cells were washed with PBS several times. Paraformaldehyde solution (4%) was used to fix the cells. After washing with PBS several times, the nuclei of the cells were stained by Hoechst 33342 solution. Finally, the cells were photographed by fluorescence microscopy to record the photothermal therapeutic effects of the nanospheres.

4T1 mouse breast cancer cells (5×10^4) were seeded in 24-well plates in 1 mL of culture media. A volume of 200 μL PB nanosphere-embedded hydrogel or blank hydrogel was added to the upper transwell (8 μm). The cells were incubated at 37 °C for 24 h. The hydrogel-containing transwells were exposed to an 808 nm laser (1 W/cm^2) for 3 min and the cells treated with blank hydrogel and the cells that did not receive NIR treatment were used as controls. Finally, the cells were treated and pictured as the above section.

2.4. Retention of the hydrogels around tumor tissue

The study was approved by Ethics Committee of Guangzhou Medical University (Guangzhou, China).

The near infrared fluorescent dye DiR-labeled hydrogel was prepared by adding DiR ethanol solution (100 μg/mL) to the blank hydrogel with stirring in an ice bath to make the final concentration of 2 μg/mL. The control DiR solution was prepared by adding DiR ethanol solution (100 μg/mL) to PBS with stirring to make the same final concentration of 2 μg/mL before use.

At day 0, BALB/c mice (female, 6–8 week old) were administered subcutaneously 1 million 4T1 cancer cells to establish an armpit tumor-bearing mouse model. At day 10, 500 μL of DiR-labeled hydrogel was peritumorally injected. Mice that received 500 μL of the DiR solution were used as controls. Then at different time intervals the DiR signals were captured at 740/820 nm to image the retention of hydrogel around tumor tissue (Berthold).

2.5. In vivo anti-cancer performance

At day 0, BALB/c mice (female, 6–8 week old) were administered subcutaneously 1 million 4T1 cancer cells to establish an armpit tumor-bearing mouse model. At day 7, the volume of the tumor reached approximately 200 mm^3 according to Eq. (2):

$$\text{Volume} = \text{Length} \times (\text{Width})^2/2 \quad (2)$$

At this point, 500 μL of the PB nanosphere-loaded hydrogel was administered by peritumoral injection. Mice received 500 μL of the blank hydrogel or the PB nanodispersions were used as controls. After 2 h the tumors were exposed to the 808 nm laser at 1 W/cm^2 for 5 min after the mice were anesthetized. Temperatures of the tumor tissues were recorded by an infrared imaging camera. NIR treatment was carried out every day from then on. At day 15, the mice were killed and the tumors of the test and control groups were photographed and weighed. The tumor samples were made into paraffin sections and H&E stained. Body weight of the mice was measured every day. The main organs of the mice were also sliced and H&E stained to evaluate the toxicity of the treatment.

2.6. Elimination of the PB nanospheres

Healthy mice were *i.v.* treated with 200 μL of the PB nanodispersion in saline. Four hours later, urine was collected and nanoparticles measured by the particle sizing system (Malvern, UK). The original PB nanodispersions and urine of the untreated mice were used as controls.

2.7. Statistical analysis

All values were expressed as mean ± standard deviation (SD). All comparisons were performed by the two-tailed Student's t test. A P-value less than 0.05 was taken as statistically significant and a P-value less than 0.01 was considered to be highly significant.

3. Results and discussions

3.1. Characteristics of the PB nanospheres

The PB nanoplatform was prepared by a simple one-pot synthesis. PVP was used as the stabilizer of the nanodispersions due to its favourable hydrophilicity. The final product appeared to be a blue nanodispersion and the concentration of the nanoplatform could be adjusted by dilution by adding pure water.

Fig. 2A shows that PB existed as nanospheres in the solution, with a diameter of approximately 150 nm. Particle size of the nanospheres was further validated by a particle sizing system (Fig. 2B), which shows a single peak around 315 nm. As the particle sizing system measured the hydrodynamic diameter instead of the static diameter, the latter figure was much bigger than the particle size revealed by TEM. The appearance and size of the PB nanospheres was in accordance with other reports[24].

The stability of PTA in the body fluids is vital for its performance *in vivo*. To assess the stability of the PTA, the particle size of the PB nanospheres exposed to 10% blood serum for 3 days at 37 °C was compared to that of the original sample. The sample exhibited a slight increase in diameter from 315 to 355 nm after serum exposure for 3 days at 37 °C (Fig. 2B). The increase can be explained by the serum adsorption onto the outer wall of the nanospheres. The similar diameters indicated the outstanding stability of the PB nanospheres in body fluids and, as a result, promising photothermal performance *in vivo*.

Fig. 2 C and D shows the thermo-photographs and heating curves of the PB nanospheres with serial concentrations of 100, 200, and 400 μg/mL upon 808 nm laser exposure. The PB nanospheres exhibited a dramatic increase in temperature upon NIR irradiation at any concentration. Moreover, the temperature rises along with the increase in concentration, with the final temperature of the three concentrations reaching 48.6, 55.4, and 57.7 °C. Meanwhile, the NIR exposure had little influence on the pure water control, with the control showing negligible temperature changes. The above results demonstrate the favorable photothermal effects of the PB nanospheres.

Photothermal stability is one of the most important indices to assess PTA. Indocyanine green (ICG), a typical PTA belonging to the cypates, shows severe light-bleaching and reduced photothermal efficacy after repeated NIR exposure[25,26]. Despite its excellent photo–heat conversion ability, this photothermal instability hampered the practical use of ICG as a PTA. As the PB nanosphere-loaded hydrogel would be locally administered, it was hoped that the PTA in the formed hydrogel would be able to exert long-term therapeutic effects. Fig. 2E shows the heating curve of the PB nanospheres upon repeated NIR irradiation. The nanodispersion could be re-heated to about 60 °C after 5 min laser exposure once the sample cooled to room temperature. In other words, the heating curve of each cycle was identical to the others, with the highest temperature of each cycle nearly 60 °C, and the heating curve showed negligible changes after repeated laser exposure. These data indicate that the PB nanospheres displayed satisfactory photothermal stability. To further validate this feature, the visible absorption curve and particle size of the nanospheres before and after 5-cycle NIR irradiation were measured. The NIR is considered to be biologically compatible due to its deep tissue penetration and negligible influence on tissues. PTAs are able to convert the light to heat to yield anti-cancer effects by generating an intolerable high temperature microenvironment for malignant cells. The light–heat conversion ability of the PTAs can be indicated by the visible absorption curve. The visible absorption curve in Fig. 2 F saw a steady increase from 500 to 700 nm, followed by a terrace from 700 to 800 nm, implying the encouraging NIR absorption capacity. Fig. 2 F also shows that the two visible absorption curves of the nanospheres before and after repeated laser exposure were obviously identical, with minor variations. Fig. 2 G shows that the particle size of the sample post-NIR treatment was comparable to that of the sample before NIR treatment (approximately 315 nm). Both graphs further support the encouraging photothermal stability of the PB nanospheres. Based on these results, it is estimated that the PTA would maintain the therapeutic effects throughout the retention period *in vivo* and would not be destroyed by body fluids or repeated laser exposure.

3.2. Features of the PB nanosphere-loaded Pluronic F127 hydrogel

In order to reduce the systemic toxicity of intravenously administered PTA and overcome the possible problem of unsatisfactory photothermal therapeutic effects due to the limited enrichment of the PTA in tumor tissues, thermosensitive *in situ* hydrogel was employed to encapsulate the PB nanospheres, which would be peritumorally injected. It was believed that the injectable hydrogel would solidify locally and form a semisolid hydrogel surrounding the tumor tissue, and might exhibit a long retention time. Meanwhile, the local administration would decrease systemic toxicity and improve the therapeutic outcome. In this section, the *in vitro* characteristics associated with the above aims are discussed in detail.

The PB nanosphere-embedded hydrogel was prepared by a simple one-pot method of dissolving Pluronic F127 in the nanodispersions directly. Fig. 3A shows the shape characteristics of the blank hydrogel and the PTA-containing hydrogel. It can be seen from the graph that the blank hydrogels had a highly macroporous network structure, with the pores about 50–200 μm in diameter, while the PB hydrogel exhibited a highly macroporous multi-layer structure. In detail, the blank hydrogel shows more and larger pores than the PB nanosphere-containing hydrogel. With 5000-fold magnification, the blank hydrogel displayed a smooth surface, while the surface of the PB nanosphere-containing hydrogel was noticeably rough. Actually, there were nanoparticles dispersed in the hydrogel matrix as indicated by the black arrows. The nanoparticles were about a hundred nanometers in diameter, corresponding well to the size of the PB nanospheres. It is assumed that the PTA dispersed evenly in the hydrogel matrix.

Ideally, the PB nanosphere-embedded hydrogel would exhibit pronounced photothermal performance. Fig. 3B and C show the temperature changes of the PTA-encapsulated hydrogel and the blank control hydrogel upon 808 nm laser exposure. The temperature of the PB hydrogel increased dramatically to 60.2 °C upon NIR irradiation. The heating curve of the PB hydrogel shown in Fig. 3C was comparable to that of the nanodispersions illustrated in Fig. 2D. Moreover, the laser exposure had little influence on the blank hydrogel, with negligible temperature changes throughout the period. These data indicate that the encapsulation in hydrogel did not negatively influence the photothermal performance of the PB nanospheres, and the nanosphere-loaded hydrogel was shown to display excellent photo–heat conversion transition capacity *in vivo*.

To improve the compliance of patients, non-invasive treatment is highly desired. Injectable hydrogel is one of the most widely used non-invasive administration routes. Pluronic F127

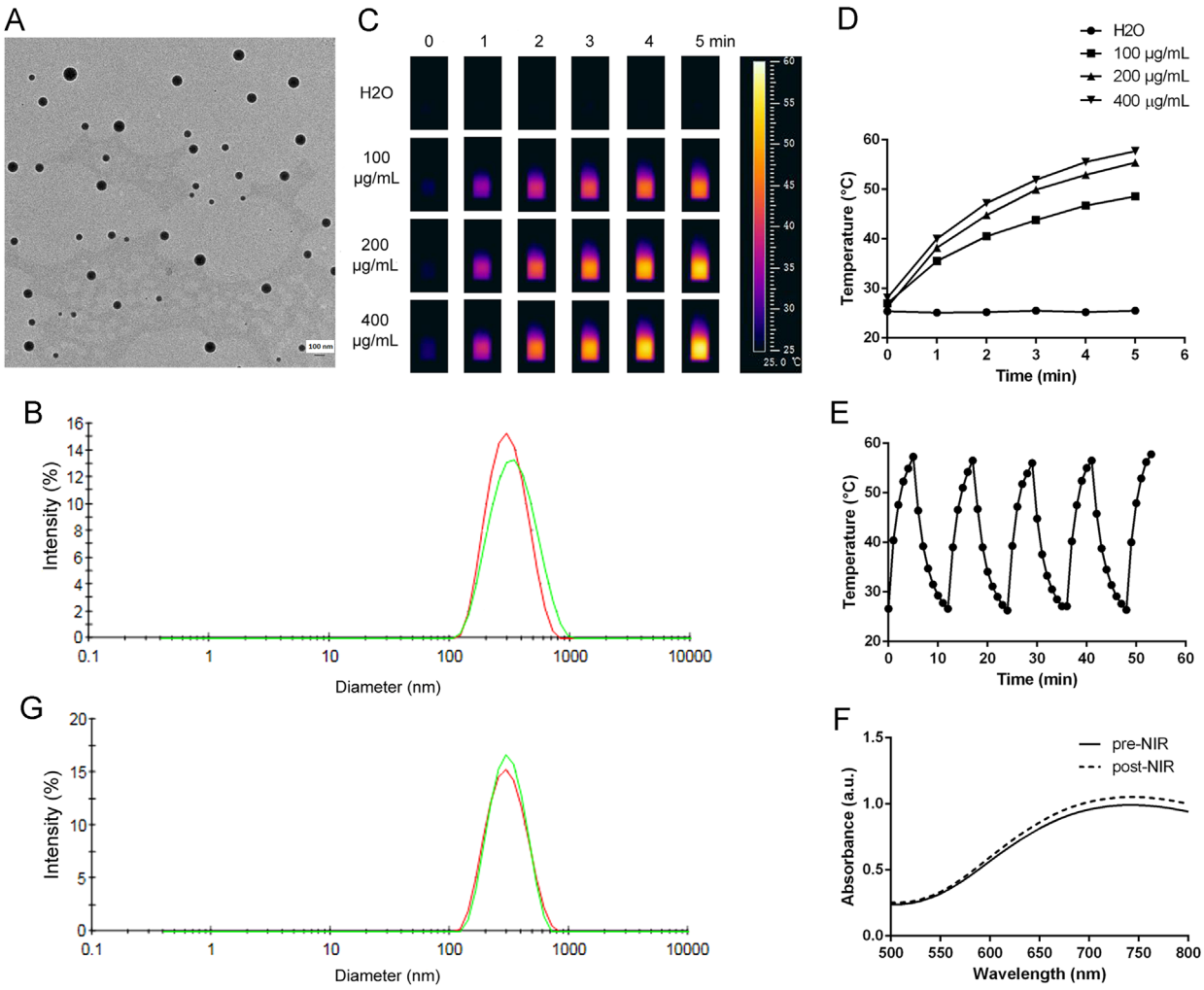

Figure 2 *In vitro* characterization of the PB nanospheres. (A) TEM image of the PB nanospheres (the scale bar represents 100 nm); (B) particle sizes of the PB nanospheres before (red) and after 3-day incubation in serum at 37 °C (green); (C) and (D) the thermographs and corresponding heating curves of the PB nanospheres at varied concentrations upon 808 nm laser exposure (1 W/cm^2); (E) the heating curves of the PB nanospheres upon repeated 808 nm irradiation (1 W/cm^2); (F) the visible absorption profiles of the PB nanospheres before and after 5-cycle 808 nm irradiation (1 W/cm^2); (G) particle sizes of the PB nanospheres before (red) and after (green) 5-cycle 808 nm irradiation (1 W/cm^2).

is a commercially available thermosensitive hydrogel. Fig. 3D shows that both the blank hydrogel and the PB hydrogel are liquid at 4 °C, and the two hydrogels changed into semisolid at body temperature. In other words, the formed *in situ* hydrogel maintained its fluidity at low temperature (< 20 °C), and the fluidity provided the injectable feature of the hydrogel. At the same time, the *in situ* hydrogel solidifies at body temperature, and the semisolid state would promise a long retention time *in vivo*. To explain the phase transition of the hydrogels in detail, the rheological characteristics of the hydrogels were studied. Fig. 3E shows the complex viscosity of the blank hydrogel and the PB hydrogel. Both of the curves exhibited a similar sharp increase in the complex viscosity in a narrow temperature range. In detail, the complex viscosity profile of the blank hydrogel showed a phase transition temperature of 30 °C, while the incorporation of the PB nanospheres resulted in a tiny increase in the phase transition temperature to 31 °C. Normally, loading water-soluble substances will increase the phase transition temperature of the hydrogel, while embedding water-insoluble agents will decrease the phase transition temperature. Despite the water-soluble PVP in the nanospheres, the PB core was water-insoluble and hydrophobic. The balance between the hydrophilicity of the PVP and the hydrophobicity of the PB core resulted in a limited change in the phase transition temperature of the hydrogel after the PB nanospheres encapsulation. These data indicate that the PB hydrogel would undergo a phase transition process after being locally administered, yielding a long retention time *in vivo*. The Pluronic F127 hydrogel will melt at a high temperature due to another phase transition. Specific to the PB hydrogel, the transition point is 54 °C. This means that the PB hydrogel would melt when the temperature reaches 54 °C upon laser exposure. But it is assumed that the phenomenon would not negatively influence the therapeutic effects *in vivo* as the PB hydrogel would quickly re-solidify once the laser expose was removed.

One of the advantages of the injectable hydrogel in treating cancers is the sustained therapeutic efficacy. To achieve this, the PTA in the hydrogels must be stable for a considerable period. In this study, the particle size and the heating curve of the PB

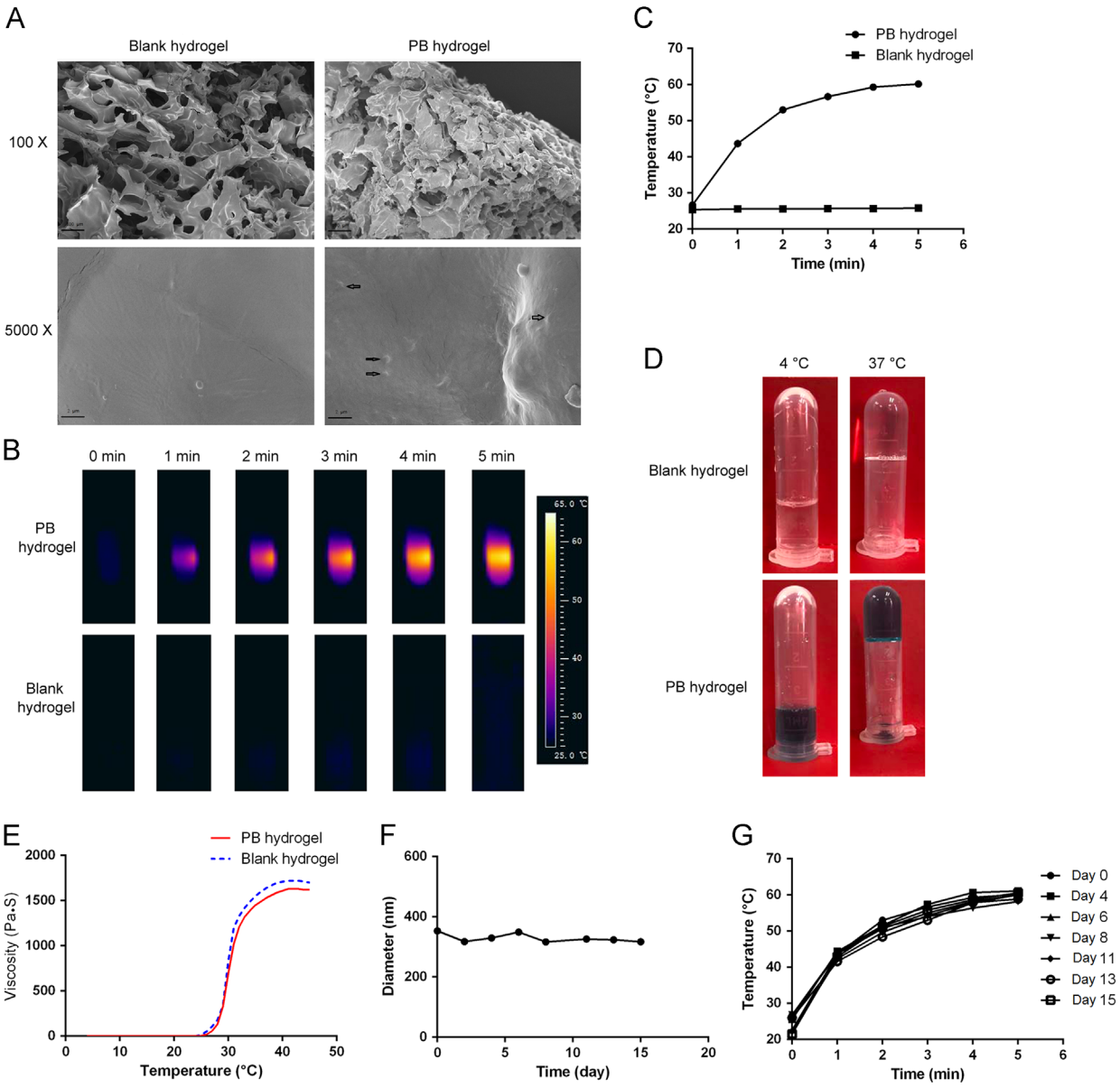

Figure 3 *In vitro* characterization of the PB hydrogel. (A) SEM images of the blank Pluronic F127 hydrogel and the PB nanosphere-loaded hydrogel (the scale bars in the upper and lower graphs represent 100 and 2 μm, respectively); (B) and (C) the thermographs and corresponding heating curves of the PB hydrogel and blank hydrogel upon 808 nm irradiation (1 W/cm^2); (D) pictures of the blank hydrogel and PB hydrogel at 4 and 37 °C; (E) the rheology curves of the blank hydrogel and PB hydrogel; (F) particle size of the PB nanospheres embedded in the hydrogel after different storage times at 37 °C; (G) the heating profiles of the PB hydrogel upon 808 nm laser exposure (1 W/cm^2) after different storage times at 37 °C.

nanospheres after being encapsulated were measured. Fig. 3F shows that the nanospheres in the hydrogel maintained a nearly constant diameter around 320 nm, comparable to the original particle size before being loaded. The result indicates that the PB nanospheres remained stable in the hydrogel in terms of particle size. Fig. 3G shows the heating profiles of the PB hydrogel before and after storage at 37 °C for several days. It can be seen that all the heating curves were almost identical, with the temperature reaching about 60 °C at the end of laser exposure. It seems that the encapsulation and storage at body temperature had little influence on the photothermal performance of the PB nanospheres. Moreover, as all the heating profiles were obtained by recording the thermograph of the same hydrogel sample upon NIR irradiation at different time intervals, it can be concluded that the PB nanospheres remained stable in photo-heat transition ability after repeated 808 nm laser exposure. Statistically, the similarity factor f_2 between the initial heating curve and that of the 4th, 6th, 8th, 11th, 13th, and 15th day were 91.4, 82.0, 82.6, 77.9, 77.1 and 80.0, respectively. All the similarity factors f_2 are over 50, which indicates that all the heating profiles were highly comparable. Both results support the hypothesis that incorporation into the hydrogels and storage at body temperature would not negatively influence the PB nanospheres and implies that the PTA would provide sustained therapeutic effects *in vivo*.

3.3. *In vitro anti-cancer photothermal therapy*

In this section, the photothermal therapeutic effects of the PB nanospheres and the PTA-loaded hydrogel against the 4T1 mouse breast cancer cells was evaluated.

Fig. 4A illustrates the fluorescence images of the 4T1 cells, with all the cells stained blue and the dead cells stained red. As anticipated, the PBS treatment alone resulted in little cell death. Moreover, the combination of PBS treatment and 808 nm laser exposure also led to insignificant cell death, with only a few cells stained red. The results indicate that the NIR light did not have a detrimental effect on cell survival and the NIR light could be regarded as bio-safe. Furthermore, the PB nanospheres at a concentration of 50 μg/mL did not exert obvious toxicity to the cells, as indicated by the comparable extent of cell death compared to the PBS control group. The result indicated the encouraging biocompatibility of the PB nanospheres. Based on the observation, we believe that the PTA would produce tolerable side effects to healthy tissues without NIR irradiation. As anticipated, the combination of PB nanosphere treatment and 808 nm laser exposure resulted in significant cell death, with almost all the cells under irradiation failing to survive. Furthermore, the overlay image shows a clear dividing line separating the live and dead cells. The dividing line is the boundary of the laser light; only the cells irradiated by the laser light died. The presence of the dividing line points out that photothermal therapy can be carried out accurately and precisely.

To analyze the toxicity and therapeutic effects of the PB nanospheres quantitatively, an MTT test was carried out. Fig. 4C shows the 4T1 cancer cell survival rate with different treatments. When the cells were free from laser exposure and treated by the PB nanospheres for 24 h only, the viability of the cells showed a decreasing trend as the PTA concentration increases, with the survival rate declining to 82.9%, 71.9% and 69.8% at the PB nanosphere concentrations of 50, 100 and 200 μg/mL, respectively. Once the cells treated by the PB nanospheres at the same concentrations were exposed to laser light, the viability of the cells further declined to 37.5%, 9.3% and 10.0%. The NIR exposure made a statistically significant difference to the survival rate of the PB nanosphere-treated cells when the PTA concentration reached 50, 100 and 200 μg/mL. These results suggest that the PB nanosphere treatment plus the NIR irradiation would exert dramatic harm to the cancer cells and the malignant cells could be totally eliminated at a high PTA concentration. As a result, it can be anticipated that the enrichment of the PB nanospheres surrounding the tumor tissues by local administration of the PTA-containing hydrogel would provide promising therapeutic effects.

To assess the biocompatibility of the PB nanospheres, the influence of the PTA on L02 hepatic cells was measured. Fig. 4C shows that more than 90% of the cells survived after 24 h treatment with the PB nanospheres at different concentrations. The result indicates that the PTA administration was safe for the healthy cells.

In this study, a transwell was employed to examine the therapeutic effects of the PB hydrogel against 4T1 cancer cells. The transwell membrane separated the upper PTA-embedded hydrogel and the lower cells. Fig. 4B shows fluorescence images of the cells, with all the cells stained blue and the dead cells stained red. It can be seen that the blank hydrogel alone did not induce cell death, indicating the outstanding compatibility of the Pluronic F127 hydrogel matrix. Moreover, the blank hydrogel plus the laser exposure also did not produce cell death. As discussed in the above section, the NIR irradiation did not cause any changes to the hydrogel. The absence of cell death during the combination of blank hydrogel and laser exposure further proved this point. Fig. 4B also shows that the PB hydrogel alone was not harmful to the cells, with negligible number of cells stained red. It seems that, despite the same incubation time, the cells treated by the PTA-loaded hydrogel exhibited much higher survival than the cells treated with the same amount of nanospheres directly, as indicated in Fig. 4C. The difference implies that the incorporation into the hydrogel reduced the unwanted adverse effects of the PB nanospheres. It was assumed that the hydrogel matrix relieved the undesirable toxicity of the chemicals by "imprisoning" them, and provided the therapeutic effects through photo-heat conversion only. The ability to relieve the direct toxicity caused by the metals renders the hydrogel an ideal candidate to decrease the systemic toxicity of the PTA. Fig. 4B also shows that the cancer cells were almost completely eliminated when the cells were exposed to the PB hydrogel together with the NIR irradiation. Obviously, the temperature increase caused by the PB hydrogel under the laser exposure killed the malignant cells. It is worth noting that, despite the same irradiation time and strength as well as the PTA dose, the PB hydrogel produced a much larger cell death area than the free nanospheres, as indicated in Fig. 4 A. In other words, concentrated PTA provided more promising photothermal therapy than an evenly dispersed PTA of the same dose. The hydrogel not only reduced the direct chemical toxicity of the PB nanospheres, but also enhanced the photothermal therapeutic effects. The results further indicate the superiority of the hydrogel in achieving more pronounced photothermal therapy.

3.4. *Local retention of the PB nanosphere-embedded hydrogel*

In order to reduce the systemic toxicity and enhance the photothermal therapeutic effects, the PB hydrogel was peritumorally administered. It was assumed that the thermosensitive hydrogel would change into semisolid hydrogel locally, and then the encapsulated PB nanospheres would have a long retention surrounding the tumor tissues and, as a result, provide a sustained therapeutic effect after one non-invasive administration. The prerequisite of the sustained therapeutic effect is a long retention *in vivo*. To image the retention of the hydrogel *in vivo*, a near-infrared imaging technique was employed. The near-infrared fluorescence dye DiR-labeled hydrogel was used, with the DiR solution used as a control group. Fig. 5 A shows the fluorescence images of the breast tumor-bearing mice after being peritumorally treated by DiR hydrogel or free DiR solution. The free DiR-treated mice showed a rapid signal decrease, with weak fluorescence signal at day 10 and almost undetectable fluorescence signal at day 15. The rapid fluorescence signal decrease meant the rapid loss of the agent from the tumor site. At the same time, the DiR hydrogel-treated mice yielded a nearly constant fluorescence signal, with the signal strength at day 10 comparable to the original signal strength at day 0 and only a slight signal decrease at day 15. The stable fluorescence strength indicated little loss of the agent from the tumor site. In other words, the *in situ* hydrogel guaranteed a promising retention of the treating agents surrounding the tumor site and, as a result, provided the basis of the sustained therapeutic effects. Normally, the Pluronic F127 hydrogel remains in the injection site for about 5 days. But in this study, the retention

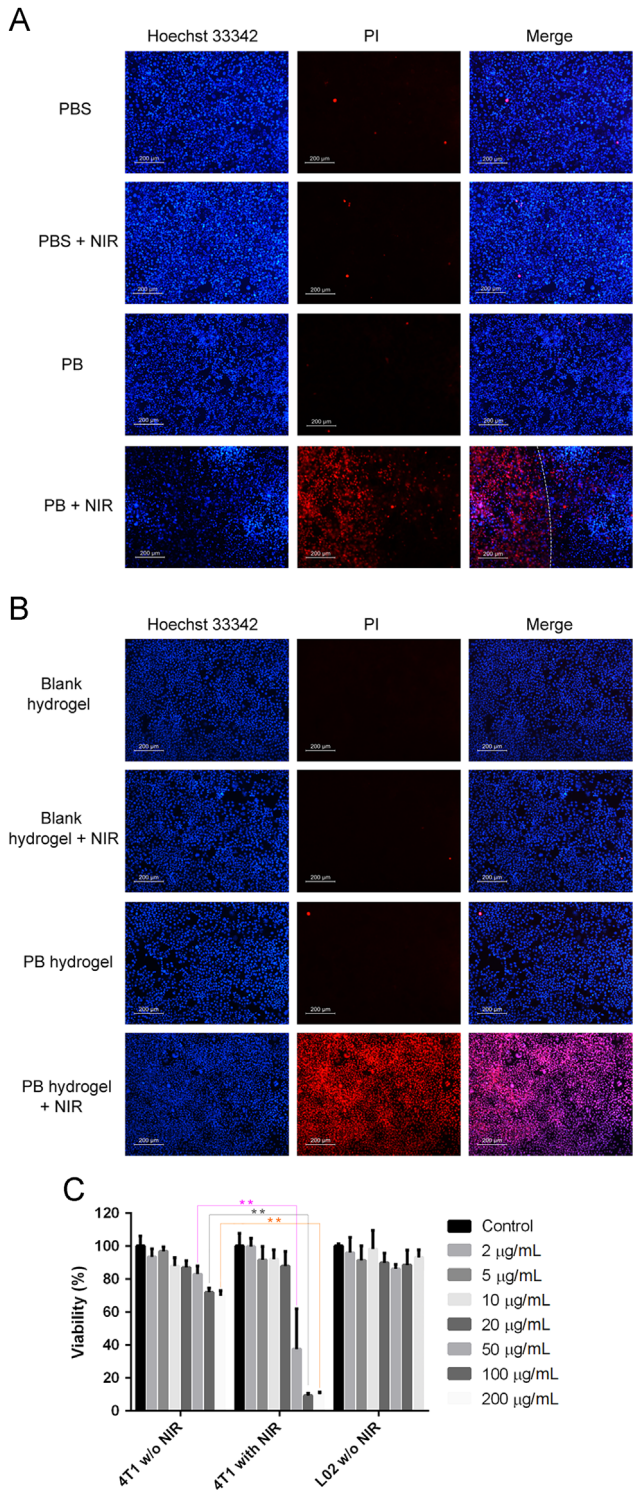

Figure 4 The anti-cancer effects of the PB nanospheres and the hydrogel against 4T1 mouse breast cancer cells. (A) The fluorescence images of the 4T1 cells after being treated by the PB nanospheres differently, the red color represents the dead cells stained by propidium iodide and the blue color represents the nucleus of all the cells; the white line is the boundary of the 808 nm laser; (B) the fluorescence images of the lower 4T1 cells after being treated by the blank hydrogel and PB hydrogel in the upper transwell, the red color represents the dead cells stained by propidium iodide and the blue color represents the nucleus of all the cells; (C) the survival rates of the 4T1 cells and the L02 cells measured by the MTT test after being treated with the PB nanospheres, $^{**}P < 0.01$. Scale bar: 200 μm.

time was much longer. The phenomenon could be explained by the special environment of tumor tissues. Due to the leaky blood vessels and the lack of lymph, tumor tissue is renowned for the enhanced permeability and retention effects. It was assumed that the enhanced retention of the PB hydrogel surrounding the tumor tissue was also ascribed to the lack of lymph.

3.5. *In vivo anti-cancer performance*

In this section, the anti-cancer performance of the PB nanosphere-embedded hydrogel was evaluated in a breast cancer-bearing mouse model, with the blank hydrogel as a control.

Fig. 5B shows the thermographs of the PB hydrogel or blank hydrogel or the PB nanodispersions peritumorally treated tumor-bearing mice upon 808 nm laser irradiation. Fig. 5C illustrates the temperatures of the tumor tissue at different time points. It can be seen that the blank hydrogel-treated mouse exhibited a moderate temperature increase at the tumor site upon the NIR exposure, with the temperature reaching 45.9 °C at the end of irradiation. The temperature increase was probably caused by the direct tissue-heating effect of the NIR. The PB nanodispersion-treated mouse exhibited a temperature increase to about 54 °C at the end of the laser expose. The PB hydrogel-treated mouse displayed a sharp temperature increase at the tumor site upon the laser exposure, with the temperature approaching 69 °C at the end of NIR irradiation. The significantly higher local temperature of the PB hydrogel-treated mouse compared to the PB nanodispersion group can be ascribed to the retention of the PTA embedded hydrogel surrounding the tumor tissues, while the free PB nanospheres were less likely to maintain a high concentration in the malignant tissues. The results indicate the outstanding photo-heat transition ability of the PTA-loaded hydrogel *in vivo*. The excellent photo–heat transition capacity is expected to provide a promising photothermal therapeutic effect against cancer.

After the NIR irradiation over eight sequential days, the tumor tissues of the test and control groups were collected, as shown in Fig. 5D. Despite the same laser strength and radiation time, the tumor samples of the blank hydrogel- and the PB solution-treated mice were obviously larger than those of the PB hydrogel-treated mice. Specifically, two mice peritumorally treated by the PB hydrogel plus the NIR irradiation were totally cured, with the tumor tissues undetectable at the end of the experiment. The tumor weights between the test and control groups were statistically different ($P < 0.05$), with the mean tumor weight of the PB hydrogel group, the PB nanodispersion group and the blank hydrogel group 0.23, 0.66 and 0.76 g, respectively, as illustrated in Fig. 5E. The tumor weights between the PB nanodispersion group and the blank hydrogel group did not show a statistical difference. The above results demonstrate the excellent photothermal therapeutic effects of the PB nanosphere-encapsulated hydrogel against cancer.

As shown in Fig. 5F, it is worth noting that, comparable to the control groups, necrosis was absent in the tumor tissue of the test group. It was estimated that the generated heat could not penetrate into the core of the tumor tissue to induce cell death; as a result, necrosis was undetectable in the remaining tumor tissue. The phenomenon indicated that the PB hydrogel provided the therapeutic effects through "burning" the cancer cells layer by layer.

3.6. *Systemic toxicity and elimination of the PB nanospheres*

To evaluate the systemic toxicity of the treatments, the body weights of the mice were measured. Fig. 6A shows that the mice

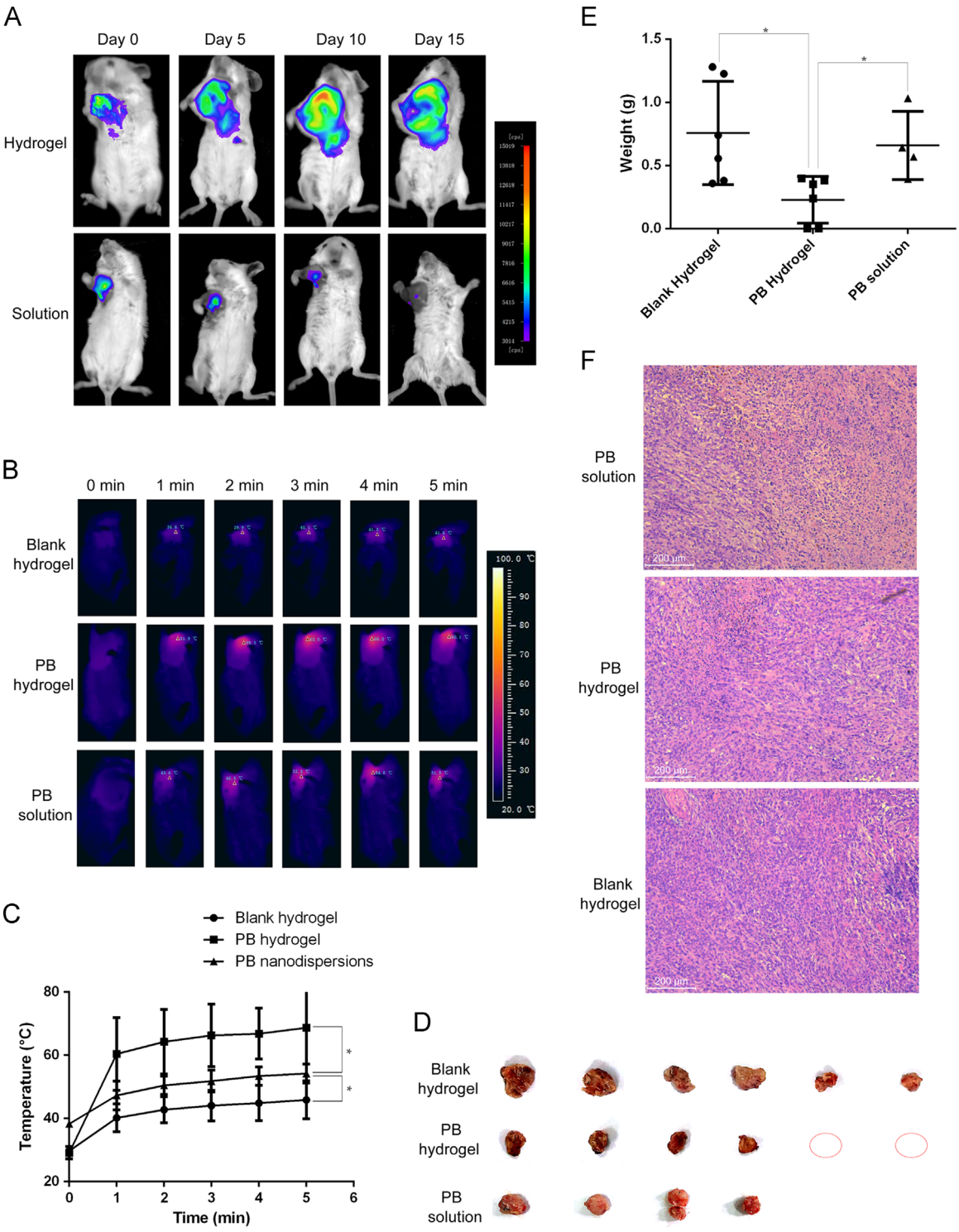

Figure 5 *In vivo* performances of the PB hydrogel in a tumor-bearing mouse model. (A) The retention of the DiR-labeled hydrogel and free DiR solution after peritumoral administration (Ex/Em: 740/820 nm); (B) and (C) the thermographs and the corresponding heating curves of the tumor sites after peritumoral administration of the blank hydrogel or PB hydrogel or the PB nanodispersions plus 808 nm irradiation (1 W/cm^2), $^*P < 0.05$; D) pictures of the tumor tissues after photothermal therapy (1 W/cm^2, 5 min) over eight sequential days, the red circle represents visibly undetectable tumor sample; (E) statistic graph of the tumor weights, $^*P < 0.05$; F) hematoxylin & eosin staining of the tumor tissues.

of three groups had a nearly constant body weight, with a small initial fluctuation probably due to the anesthesia in the first few days. The relatively stable body weight indicated that the non-invasive administration of the thermosensitive PB hydrogel plus the laser irradiation induced negligible systemic toxicity. This point was further confirmed by the tissue sections. As shown in Fig. 6B, the heart, liver, spleen, lung and kidney of the PB hydrogel-treated mice did not display abnormal morphology. In

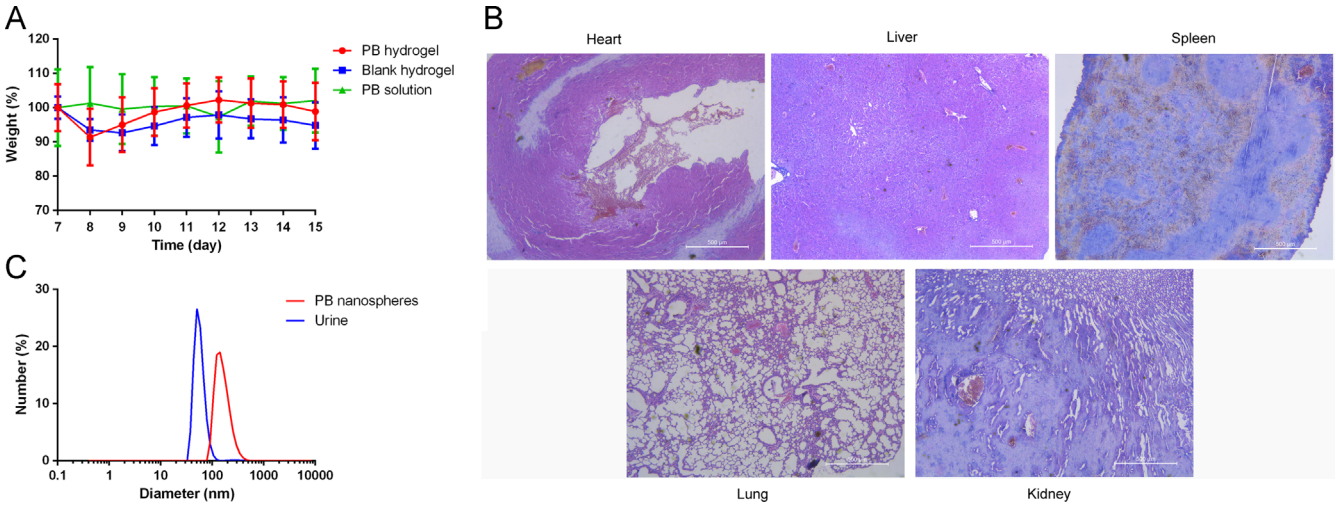

Figure 6 (A) Body weight curves of the tumor-bearing mice throughout the experimental period; (B) hematoxylin & eosin staining of the main organs of the PB hydrogel-treated tumor-bearing mouse; (C) particle sizing distribution of the PB nanospheres (red) and the urine from the PB nanodispersions i.v. treated mouse (blue).

summary, it is clear that the injectable and temperature-responsive *in situ* PB hydrogel is a promising PTA for cancer treatment with low systemic toxicity.

To investigate the possible elimination pathways of the PB nanospheres, the urine of the PB nanodispersion-treated mice was collected and measured by the particle sizing system. Fig. 6 C shows that nanoparticles of about 50 nm appeared in the urine, while similar nanoparticles were absent in the urine of the untreated mice. The observed nanoparticles were probably the PB nanospheres excreted through the urine. Particle size of the original PB nanospheres was about 110 nm, bigger than the nanoparticles in the urine. It is proposed that the PB nanospheres were processed into smaller ones and then eliminated through the urine. As a result, this likely would not induce accumulation toxicity.

4. Conclusions

In this study an injectable and thermosensitive hydrogel containing PB nanoparticles for photothermal therapy against cancer is reported. The PB particles show nanosphere structure with a diameter of about 150 nm. The nanospheres are evenly distributed in the hydrogel matrix and maintained their particle size. The PTA-loaded hydrogel showed excellent photo–heat conversion ability and outstanding repeated irradiation stability. The hydrogel not only exhibited thermo-responsive *in situ* gel-forming capacity at body temperature, but also reduced the chemical toxicity of the PB by "imprisoning" the nanospheres in the matrix. Moreover, the concentrated PTA in the hydrogel exhibited more promising therapeutic effects against cancer cells than a nanospheres solution. Lastly, the PB nanosphere-embedded hydrogel displayed pronounced tumor-curing effects after peritumoral administration due to the enhanced retention *in vivo* and elevated local temperature surrounding the tumor tissue upon the NIR exposure. The preparation shows no systemic toxicity.

Acknowledgments

The research was supported by National Natural Science Foundation of China (81803463 and 51403043), the funding from Guangzhou Medical University (Grant No. B185004204, China) and Guangzhou City Council (1201410511, China) and Guangdong Provincial Council (15KAL10, China), Munici-pal College Research Program of Guangzhou Education Bureau (1201610202, China), Guangdong Natural Science Foundation (2015A030310037, China), and Guangdong Medical Science & Technology Research Foundation (A2017069, China), and the Scientific Research Foundation of Guangzhou Education Bureau (1201610085 and 1201430509, China) and Natural Science Foundation of Guangzhou Medical University (2014C09, China).

References

1. Zhu L, Li M, Liu X, Du L, Jin Y. Inhalable oridonin-loaded poly(lactic-*co*-glycolic)acid large porous microparticles for *in situ* treatment of primary non-small cell lung cancer. *Acta Pharm Sin B* 2017;**7**:80–90.
2. Wu T, Geng J, Guo J, Gao J, Zhu X. Asiatic acid inhibits lung cancer cell growth *in vitro* and *in vivo* by destroying mitochondria. *Acta Pharm Sin B* 2017;**7**:65–72.
3. Lin M, Tang S, Zhang C, Chen H, Huang W, Liu Y, et al. *Euphorbia* factor L2 induces apoptosis in A549 cells through the mitochondrial pathway. *Acta Pharm Sin B* 2017;**7**:59–64.
4. Xia Y, Xu T, Wang C, Li Y, Lin Z, Zhao M, et al. Novel functionalized nanoparticles for tumor-targeting co-delivery of doxorubicin and siRNA to enhance cancer therapy. *Int J Nanomed* 2018;**13**:143–59.
5. Zhou Y, Wen H, Gu L, Fu J, Guo J, Du L, et al. Aminoglucose-functionalized, redox-responsive polymer nanomicelles for overcoming chemoresistance in lung cancer cells. *J Nanobiotechnol* 2017;**15**:87.
6. Li Y, Guo M, Lin Z, Zhao M, Xiao M, Wang C, et al. Polyethylenimine-functionalized silver nanoparticle-based co-delivery of paclitaxel to induce HepG2 cell apoptosis. *Int J Nanomed* 2016;**11**:6693–702.
7. Cheewatanakornkool K, Niratisai S, Manchun S, Dass CR, Sriamornsak P. Characterization and *in vitro* release studies of oral microbeads containing thiolated pectin–doxorubicin conjugates for colorectal cancer treatment. *Asian J Pharm Sci* 2017;**12**:509–20.
8. Yang RM, Fu CP, Fang JZ, Xu XD, Wei XH, Tang WJ, et al. Hyaluronan-modified superparamagnetic iron oxide nanoparticles for bimodal breast cancer imaging and photothermal therapy. *Int J Nanomed* 2017;**12**:197–206.

9. Krishnan G, Subramaniyan J, Subramani PC, Muralidharan B, Thiruvengadam D. Hesperetin conjugated PEGylated gold nanoparticles exploring the potential role in anti-inflammation and anti-proliferation during diethylnitrosamine-induced hepatocarcinogenesis in rats. *Asian J Pharm Sci* 2017;**12**:442–55.
10. Yang X, Wu S, Xie W, Cheng A, Yang L, Hou Z, et al. Dual-drug loaded nanoneedles with targeting property for efficient cancer therapy. *J Nanobiotechnol* 2017;**15**:91.
11. Dong Y, Sigen A, Rodrigues M, Li X, Kwon SH, Kosaric N, et al. Injectable and tunable gelatin hydrogels enhance stem cell retention and improve cutaneous wound healing. *Adv Funct Mater* 2017;**27**:1606619.
12. Gonzalez MA, Simon JR, Ghoorchian A, Scholl Z, Lin S, Rubinstein M, et al. Strong, tough, stretchable, and self-adhesive hydrogels from intrinsically unstructured proteins. *Adv Mater* 2017;**29**:1604743.
13. Xu L, Liang Y, Sun C, Hao N, Yan J, Gao W, et al. Substitution of percutaneous ethanol injection with a low molecular weight peptide gel mimicking chemoembolization for cancer therapy. *Nanotheranostics* 2017;**1**:313–25.
14. Lee SS, Choi GE, Lee HJ, Kim Y, Choy JH, Jeong B. Layered double hydroxide and polypeptide thermogel nanocomposite system for chondrogenic differentiation of stem cells. *ACS Appl Mater Interfaces* 2017;**9**:42668–75.
15. Li R, Liang J, He Y, Qin J, He H, Lee S, et al. Sustained release of immunosuppressant by nanoparticle-anchoring hydrogel scaffold improved the survival of transplanted stem cells and tissue regeneration. *Theranostics* 2018;**8**:878–93.
16. Wang Z, Liang C, Shi F, He T, Gong C, Wang L, et al. Cancer vaccines using supramolecular hydrogels of NSAID-modified peptides as adjuvants abolish tumorigenesis. *Nanoscale* 2017;**9**:14058–64.
17. Strassburg A, Petranowitsch J, Paetzold F, Krumm C, Peter E, Meuris M, et al. Cross-linking of a hydrophilic, antimicrobial polycation toward a fast-swelling, antimicrobial superabsorber and interpenetrating hydrogel networks with long lasting antimicrobial properties. *ACS Appl Mater Interfaces* 2017;**9**:36573–82.
18. Lin FW, Chen PY, Wei KC, Huang CY, Wang CK, Yang HW. Rapid *in situ* MRI traceable gel-forming dual-drug delivery for synergistic therapy of brain tumor. *Theranostics* 2017;**7**:2524–36.
19. Liu M, Song X, Wen Y, Zhu JL, Li J. Injectable thermoresponsive hydrogel formed by alginate-*g*-poly(*N*-isopropylacrylamide) that releases doxorubicin-encapsulated micelles as a smart drug delivery system. *ACS Appl Mater Interfaces* 2017;**9**:35673–82.
20. Huang X, Deng G, Liao L, Zhang W, Guan G, Zhou F, et al. $CuCo_2S_4$ nanocrystals: a new platform for multimodal imaging guided photothermal therapy. *Nanoscale* 2017;**9**:2626–32.
21. Yin J, Chen D, Wu S, Li C, Liu L, Shao Y. Tumor-targeted nanoprobes for enhanced multimodal imaging and synergistic photothermal therapy: core-shell and dumbbell Gd-tailored gold nanorods. *Nanoscale* 2017;**9**:16661–73.
22. Jin L, Liu J, Tang Y, Cao L, Zhang T, Yuan Q, et al. MnO_2-functionalized Co-P nanocomposite: a new theranostic agent for pH-triggered T_1/T_2 dual-modality magnetic resonance imaging-guided chemo-photothermal synergistic therapy. *ACS Appl Mater Interfaces* 2017;**9**:41648–58.
23. Jiang Q, Luo Z, Men Y, Yang P, Peng H, Guo R, et al. Red blood cell membrane-camouflaged melanin nanoparticles for enhanced photothermal therapy. *Biomaterials* 2017;**143**:29–45.
24. Zhang N, Cai X, Gao W, Wang R, Xu C, Yao Y, et al. A multifunctional theranostic nanoagent for dual-mode image-guided HIFU/chemo- synergistic cancer therapy. *Theranostics* 2016;**6**:404–17.
25. Sahu A, Lee JH, Lee HG, Jeong YY, Tae G. Prussian blue/serum albumin/indocyanine green as a multifunctional nanotheranostic agent for bimodal imaging guided laser mediated combinatorial phototherapy. *J Control Release* 2016;**236**:90–9.
26. Cheng L, Gong H, Zhu W, Liu J, Wang X, Liu G, et al. PEGylated Prussian blue nanocubes as a theranostic agent for simultaneous cancer imaging and photothermal therapy. *Biomaterials* 2014;**35**:9844–52.